A Primary Study in Adaptive Clutter Reduction and Buried Minelike Target Enhancement From GPR Data

John W. Brooks [a], Luc van Kempen[b] and Hichem Sahli[c]

[a]Brooks Enterprises International, Inc., Huntsville, AL, USA *

[b,c]Vrije Universiteit Brussel - Faculty of Applied Sciences
ETRO Dept. IRIS Research group **

ABSTRACT

This paper describes the theory and practice of ground penetrating radar (GPR) clutter characterization and removal. Clutter and target parametric and non-parametric modeling methods are described and results of these methods on laboratory data are presented. Data were collected at the Technische Universität Ilmenau (TUI) using a 6 GHz frequency-stepped GPR. Targets were chosen to include rocks and other non-lethal clutter which normally present false targets to the GPR. Results indicate a quantifiable improvement in target class discrimination using the clutter reduction methods over standard mean background removal methods.

Keywords: GPR, antipersonnel land mine, feature extraction, system identification

1. INTRODUCTION

Anripersonnel landmines (APLs) remain hidden in the ground in over 64 countries following the termination of armed conflict.[1–3] The exact number of APLs is not known[4]; indeed, the actual number of APLs is rathr irrelevant. The fact remains that APLs account for hundreds of civilian casualties per year and prevent the return of land to agricultural use The standard approach to the detection of APLs remains the metal detector (MD) which is essentially unchanged from the approach used in World War II. Because a large number of APLs contain little to no metal, ground penetrating radar (GPR) is one of the current technologies which is receiving attention as an alternative or adjunct to the metal detector. The r requirement for reliable land mine detection from a stand-off location is applicable for both military and humanitarian (post-conflict) applications. Comprehensive reports on current research in APL detection/classification are found in the proceedings of the First and Second EUREL International Conferences on the Detection of Abandoned Land Mines in Edinburgh, Scotland, in October 1996 and October 1998,[5,6] and the proceedings of the October 1997 conference on Sustainable Humanitarian Demining (SusDem '97) held in Zagreb, Croatia.[7] SPIE, the International Society for Optical Enginering has held four conferences on demining technology[8–11]; over 250 papers are contained in those volumes covering all aspects of mine detection technologies.

2. CLUTTER CHARACTERIZATION

GPR clutter includes many components; crosstalk from transmitter to receiver antenna, initial ground reflection and background resulting from scatterers within the soil. In this paper, all of these components are considered to be undesired signals which require estimation and subsequent removal in order to enhance the target signal. As mentioned previously, the target signal can be either a mine or non-mine; it is the objective of the post-processing to make the decision between the two.

System Identification methods[12] offer considerable promise in GPR signal processing. One goal of system identification is to attempt to determine a target impulse response which will be invariant with aspect angle and soil conditions. In general, this will not be possible.[13,14] Aspect-invariant impulse responses, characterized by the natural resonant poles of the system, are valid only when the target is perfectly conducting and in free space.

Further author information:
(*)1509 Locust Circle, S.E., Huntsville, AL 35801, USA; email: jbrooks@hiwaay.net, Phone/Fax: +1-256-539-0148
(**)Pleinlaan 2, B-1050 Brussels - Belgium, Tel: ++32-2-6292916 - Fax: ++32-2-6292883,{lmkempen,hsahli,jpcornel}@etro.vub.ac.be

2.1. The GPR Signal Model

Estimating the target parameters is the goal of system identification applied to GPR signal processing. If specific parameters of the target can be isolated in some domain, then it may be possible to separate the target further into "Mine" and "Non-Mine" classes. The roots of the transfer function polynomials may be plotted in either the *z*-domain or the *s*-domain, and an appropriate distance function can be applied to separate the target sets. Figure 1 shows the basic structure of the input-output relationship is between the transmitted signal and the received signal. From this diagram,

$$s_{rec'd}(n) = s_{trans}(n) * h_a(n) * h_c(n) * h_t(n) * h_c(n) * h_a(n) \tag{1}$$

where $h_a(n)$,$h_c(n)$ and $h_t(n)$ are the impulse responses of the antenna, clutter and target, respectively. The symbol $*$ denotes linear convolution, defined as

$$u(n) * h(n) := \sum_{k=-\infty}^{\infty} h(k)u(n-k). \tag{2}$$

The antenna and clutter impulse responses are shown twice to reinforce the fact that the radar wave passes through both components twice. Strictly speaking, in a bistatic array environment, the antenna impulse responses should be denoted $h_{a_{rec}}(n)$ and $h_{a_{trans}}(n)$ to denote the receiver and transmitter antenna responses which will, in general, be different.

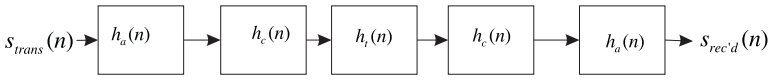

Figure 1. Overview of System Impulse Response

2.2. Model-Based Parametric System Identification

Under ideal circumstance, Eq. 1 implies that the target impulse response should be obtainable by deconvolving the various components of the received signal, but, in general, this is not feasible.[15]

Consider a discrete LTI system described by the difference equation

$$y(n) + a_1 y(n-1) + a_2 y(n-2) + \cdots + a_{n_a} y(n-n_a) = b_0 u(n) + b_1 u(n-1) + \cdots + b_{n_b} u(n-n_b) \tag{3}$$

where $y(n)$ is the output sequence and $u(n)$ is the input sequence, and n_a,n_b represent the order of the output and input processes, respectively. For causality, $n_b \leq n_a$. The system described by 3 may be written in transfer function format as

$$H(z) = \frac{B(z^{-1})}{A(z^{-1})} \tag{4}$$

where

$$A(z^{-1}) = 1 + a_1 z^{-1} + a_2 z^{-2} + \cdots + a_{n_a} z^{-n_a} \tag{5a}$$
$$B(z^{-1}) = b_0 + b_1 z^{-1} + b_2 z^{-2} + \cdots + b_{n_b} z^{-n_b} \tag{5b}$$

This system has the following representation:

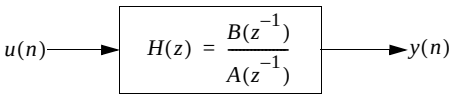

Figure 2. Discrete LTI Block Diagram

The more general case includes additional measurement noise $e(n)$ which is assumed to be i.i.d. with mean zero. In this case, the input-output relation is written

$$A(z^{-1})y(n) = B(z^{-1})u(n) + e(n) \tag{6}$$

which is the *equation-error* in system identification language.[12] Define the *parameter vector* $\boldsymbol{\theta}$ as

$$\boldsymbol{\theta} = [a_1, a_2, \ldots a_{n_a}, b_0, b_1, \ldots b_{n_b}]^T \tag{7}$$

and the elements of this vector are the parameters to be estimated. Let

$$\boldsymbol{x}^T(k) = \left[-y(k-1), \quad \ldots, -y(k-n_a), \quad u(k), \quad \ldots, u(k-n_b)\right]$$

then

$$y(k) = \boldsymbol{x}^T(k)\boldsymbol{\theta} + e(k) \tag{8}$$

or

$$\boldsymbol{y} = X\boldsymbol{\theta} + \boldsymbol{e} \tag{9}$$

where X is the matrix

$$X = \begin{bmatrix} \boldsymbol{x}^T(n+1) \\ \boldsymbol{x}^T(n+2) \\ \vdots \\ \boldsymbol{x}^T(n+N) \end{bmatrix} = \begin{bmatrix} -y(n_a), & \ldots, & -y(1), & u(n_b+1), & \ldots, & u(1) \\ -y(n_a+1), & \ldots, & -y(2), & u(n_b+2), & \ldots, & u(2) \\ \vdots & \ddots & & \vdots & \ddots & \\ -y(n_a+N-1), & \ldots, & -y(N), & u(n_b+N), & \ldots, & u(N) \end{bmatrix} \tag{10}$$

where N is the length of a sliding data window; $N \gg n_a + n_b$.

It is shown in Ref. 16 that the solution of Eq. 9 is given by the minimum-norm

$$\hat{\boldsymbol{\theta}} = (X^T X)^{-1} X^T \boldsymbol{y} = X^\dagger \boldsymbol{y} \tag{11}$$

where $X^\dagger$ is the *Moore-Penrose Pseudo-inverse*[17] of X.

Fig. 3 is a general block diagram of the three main components of the received signal. Estimated parameters may be used for feature extraction and clutter reduction.

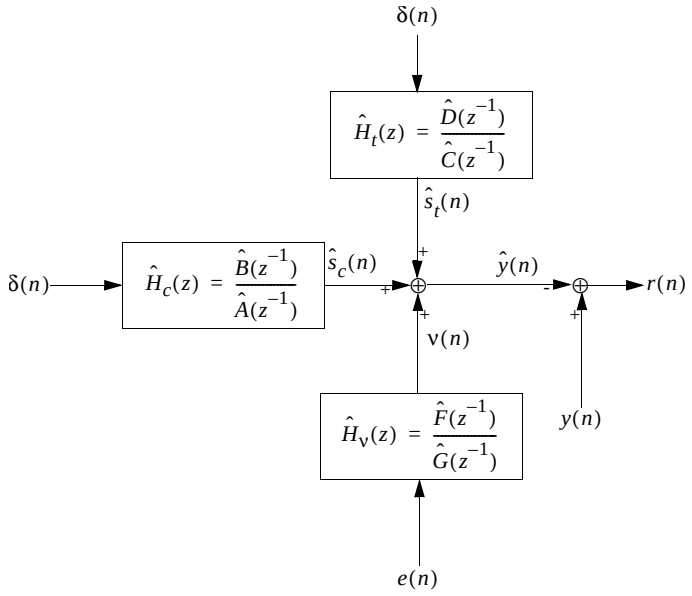

Figure 3. General Block Diagram Representation of System Identification

2.2.1. The Target Model

The target model is shown in Fig. 4. The impulse response of the target is $h_t(n)$, and the input-output relationship is as shown, with a Dirac δ-function as the input, and the output sequence by $\hat{s}_t(n)$. As stated previously, the goal will be to estimate the parameters of the transfer function, $\hat{D}(n)$ and $\hat{C}(n)$ given by the composite parameter vector

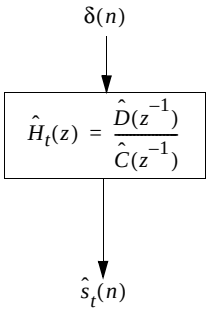

Figure 4. Representation of Target Parametric Model

$$\hat{\boldsymbol{\theta}}_t = [c_1, c_2, \ldots c_{n_c}, d_0, d_1, \cdots d_{n_d}]^T \tag{12}$$

where n_c,n_d represent the order of the respective polynomials in z^{-1}.

The parameters of the target may be estimated only after the clutter/antenna parameters are determined.

2.2.2. The Clutter Model

In a similar way, the clutter model may be represented by

$$\hat{\boldsymbol{\theta}}_c = [a_1, a_2, \ldots a_{n_a}, b_0, b_1, \cdots b_{n_b}]^T \tag{13}$$

and the block diagram is shown in Fig. 5.

The input to the clutter block diagram is indicated by the δ-function in the absence of any knowledge of the true input waveform. In this way, the clutter model includes all of the effects noted in Sect. 2. In general, the shape of the transmitted pulse will not be known. Indeed, as with the data collected at TUI, there is no "pulse" *per se*, but only a synthesized pulse by virtue of the stepped frequency modulation. The modeling methods described in this section, however, lend themselves equally well to the case where the input (transmitted) pulse is known; simply replace the δ-function with the known pulse.

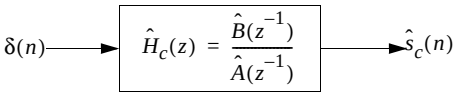

Figure 5. Representation of Clutter Parametric Model

2.2.3. The Noise Model

When modeling dynamical systems or signals, it is usually necessary to include a noise model which will account for any random disturbances caused by the measurement equipment, etc. Such disturbances may be non-stationary, and may also be non-Gaussian and display some specific spectral characteristics other than a flat ("white") spectrum. The inclusion of a (possibly time-varying) noise model is therefore indicated.

Such a noise process model can be described by

$$\hat{\boldsymbol{\theta}}_\nu = \left[g_1, g_2, \ldots g_{n_g}, f_0, f_1, \cdots f_{n_f}\right]^T \tag{14}$$

and the model is shown in Fig. 6.

The input to the noise model is a vector of independent, identically distributed (i.i.d.) samples with a Gaussian amplitude distribution of zero mean and constant spectral intensity. The input is applied to a filter which will provide appropriate spectral and amplitude shaping to represent the measured noise from A-Scan to A-Scan; it may not be necessary to apply this filter if the noise from A-Scan to A-Scan is sufficiently decorrelated.

For a general description of the parametric system identification algorithms described in this paper, reference is made to Fig. 3 and the additional figures immediately following. The clutter model is estimated by applying the Steiglitz-McBride Algorithm

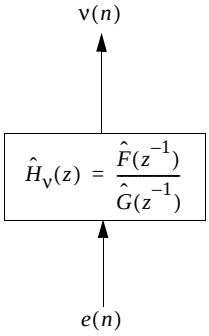

Figure 6. Representation of Added Noise Parametric Model

to a measured clutter sample with a Dirac δ-function as the input, as in Fig. 5. The clutter model is derived from a reference clutter sample, as is the case in all the techniques described herein except for some types of recursive (adaptive) methods which will be described in Sect. 2.3. This should not, in most cases, be a drawback to the general method; representative clutter samples may be collected at various times during the mine scanning process.

The noise model shown in Fig. 6 is estimated by determining the ARMA parameters of the residue found by subtracting successive A-Scans and then using those coefficients to create correlated noise samples $\nu(n)$ which are of appropriate amplitude to match the power of the original residue. It has been experimentally determined that, with the data samples of interest here, the noise transfer function may be omitted; in other words, the scan-to-scan noise is closely approximated by the input $e(n)$. If an examination of the correlation properties of the differenced A-Scans determine that the residue had significant correlations at lags much greater than zero, it would be necessary to determine the noise model ARMA parameters as, for example, described in Ref. 18. That reference uses higher-order statistics (cumulants) to determine ARMA parameters assuming the data is correlated and possibly non-Gaussian. Other ARMA estimation methods may be used, such as those in Ref.12 if the process is found to be linear and Gaussian. In practice, it was found that WGN was a close approximation to the true process; in no case was an ARMA model greater than ARMA(4,4) determined to be of use.

Once the clutter estimate and noise processes are determined, the target model may be extracted by simply subtracting the sum of those estimates from the measured signal. If desired, the target filter coefficients may be easily determined by the Steiglitz-McBride algorithm applied to the new target estimate signal as for the clutter signal described above.

2.3. Recursive (Time-Varying) Methods

Recursive algorithms, also known as *adaptive algorithms*,[12,19] are used for *on-line processing* of data as opposed to *batch or off-line processing*.

Consider

$$y(n) = \boldsymbol{x}^T(n)\boldsymbol{\theta}(n) + e(n) \tag{15}$$

The general expression for recursive parameter estimation is

$$\hat{\boldsymbol{\theta}}(n) = \hat{\boldsymbol{\theta}}(n-1) + \boldsymbol{k}(n)\,(\boldsymbol{y}(n) - \hat{\boldsymbol{y}}(n)) \tag{16}$$

where $\boldsymbol{k}(n)$ is the *adaptation gain vector*. Given an initial parameter vector

$$\boldsymbol{\theta}_0(n) = \boldsymbol{\theta}_0(n-1) + \boldsymbol{w}(n) \tag{17}$$

where $\boldsymbol{w}(n)$ is assumed to be i.i.d., the general algorithm for recursive parameter estimation is therefore

$$\hat{\boldsymbol{\theta}}(n) = \hat{\boldsymbol{\theta}}(n-1) + \boldsymbol{k}(n)\left[y(n) - \hat{y}(n)\right] \tag{18a}$$

$$\hat{y}(n) = \boldsymbol{x}^T(n)\hat{\boldsymbol{\theta}}(n-1) \tag{18b}$$

$$\boldsymbol{k}(n) = \boldsymbol{Q}(n)\boldsymbol{x}(n) \tag{18c}$$

$$\boldsymbol{Q}(n) = \frac{\boldsymbol{P}(n-1)}{R_2 + \boldsymbol{x}^T(n)\boldsymbol{P}(n-1)\boldsymbol{x}(n)} \tag{18d}$$

$$\boldsymbol{P}(n) = \boldsymbol{P}(n-1) - \frac{\boldsymbol{P}(n-1)\boldsymbol{x}(n)\boldsymbol{x}^T(n)\boldsymbol{P}^T(n-1)}{R_2 + \boldsymbol{x}^T(n)\boldsymbol{P}(n-1)\boldsymbol{x}(n)} + \boldsymbol{R}_1 \tag{18e}$$

where $\boldsymbol{R}_1 = E[\boldsymbol{w}(n)\boldsymbol{w}^T(n)]$ and R_2 is the variance of the innovations in Eq. 15, $R_2 = E[e^2(n)]$. This is the *Kalman Filter* version of adaptive parameter identification. The covariance matrix $\boldsymbol{P}$ is typically initialized as a diagonal matrix of dimension $N \times N$, where $N = n_a + n_b$ as in Eq. 3, for example.

Often, a modification to the above equations is made to include a *forgetting factor* $\{\lambda : 0 < \lambda \leq 1\}$, in which case Eq.s 18d and 18e become, respectively,

$$\boldsymbol{Q}(n) = \frac{\boldsymbol{P}(n-1)}{\lambda + \boldsymbol{x}^T(n)\boldsymbol{P}(n-1)\boldsymbol{x}(n)} \tag{19a}$$

$$\boldsymbol{P}(n) = \left[\boldsymbol{P}(n-1) - \frac{\boldsymbol{P}(n-1)\boldsymbol{x}(n)\boldsymbol{x}^T(n)\boldsymbol{P}^T(n-1)}{\lambda + \boldsymbol{x}^T(n)\boldsymbol{P}(n-1)\boldsymbol{x}(n)}\right] \diagup \lambda \tag{19b}$$

Typical values for λ range from 0.95 to 0.99.

3. RESULTS

This section describes the results of applying both common mean background removal and adaptive (RLS) background removal as described above. The data was collected at the Technische Universität Ilmenau (TUI) under the direction of Prof. Jürgen Sachs as part of the EU DEMINE Program. The stepped-frequency data was collected by dwelling at a particular position in a grid and sweeping from 0 to 6 GHz in 15 MHz steps, for a total of 401 frequency samples per A-Scan. Each target was buried such that the top of each target was 5.0cm below the surface of the sand. The sandbox is approximately 2.2 m long and 0.75 m wide. This permits up to four separate targets to be placed in such a manner to ensure at least 50 cm spacing between the targets. The frame for mounting the antennas is attached to the ceiling of the laboratory. Two carriages for the receive and transmit antennas may be moved independently in one direction. The antennas are in a bistatic configuation and may be rotated to obtain all combinations of horizontal, vertical and cross-polarizations.

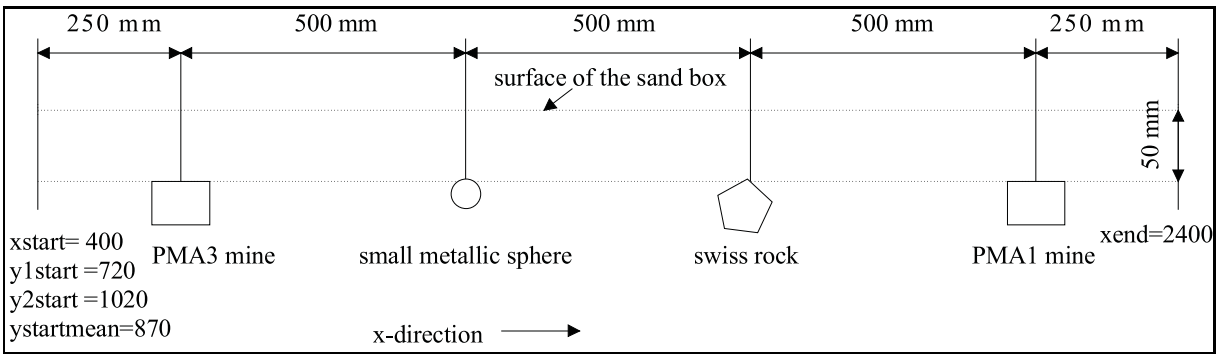

Figure 7. Measurement Scenario at TUI Lab

3.1. Summary of Clutter Reduction Methods

3.1.1. Model-Based and RLS Background Removal

Figure 8 shows the result of the clutter and noise estimation described in Sect. 2.1. In this figure, the far right side has been removed to eliminate the reflections from the wall of the sandbox. It is seen that the correlated clutter represented normally by waves below the targets, is suppressed. In this way, the dominant returns are only the tops of the targets. The noise model was estimated by differencing consecutive A-scans and evaluating the autocorrelation properties in order to establish the ARMA model order. Then, WGN was applied to the noise process transfer function shown in Fig. 6. The clutter process was estimated by applying the Dirac delta function to the clutter transfer function of Fig. 5 and experimentally determining the appropriate model by applying the Steiglitz-McBride algorithm to a clutter A-scan sample. In this figure, the clutter parameters are fixed, but the noise parameters are updated from A-scan to A-scan.

Figure 9 shows the results of the RLS adaptive approach. In this case, the clutter parameters are again considered fixed, but the signal minus clutter residue is adaptively estimated in time (depth) as well as from A-scan to A-scan. In this figure, the sphere and rock returns are reduced, but the level of correlated clutter is more than the previous approach.

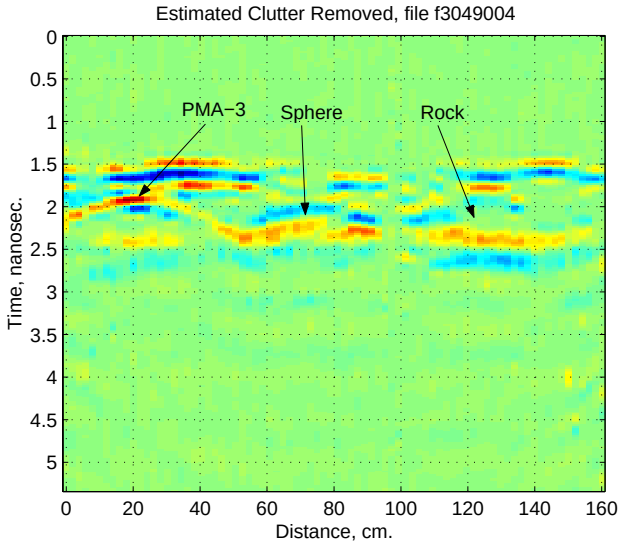

Figure 8. Parametric Model Background Removal

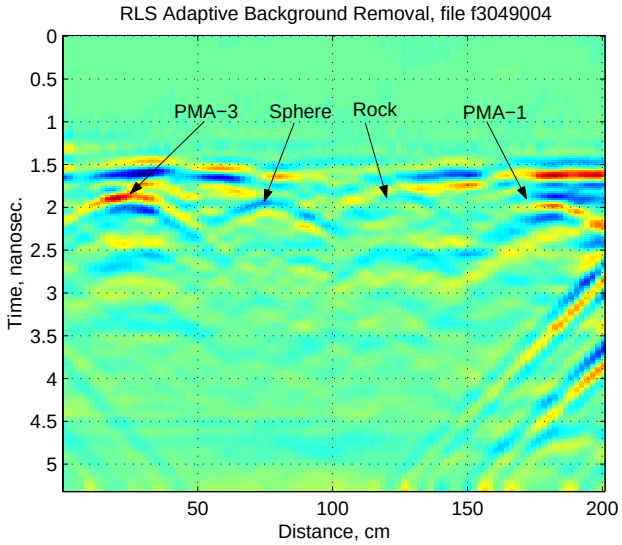

Figure 9. RLS Background Removal

3.2. Target Classification

3.2.1. Physical Parameter Estimation

An important parameter in the processing of GPR data is the knowledge of the velocity of propagation in the medium. The velocity estimation is based on the detected hyperbolas in the B-scan image. In the following the estimated hyperbolic parameters and velocities are compared for both GPR raw data (after simple average subtraction) and following clutter reduction using the adaptive method described above. The detection of target hyperbolas in the B-scans was accomplished by using a generalized Hough-transform on the detected edge pixels. Edge detection was performed using Gaussian and multi-scale Gabor filters, the details of which are in Ref. 15. The following equation for the general hyperbolic parameters was used:

$$t^2 = \alpha + \beta(x - \gamma)^2 \tag{20}$$

where t and x represent the vertical and horizontal coordinates. Figures 10 and 11 show the detected hyperbolas for the raw data before and after adaptive clutter background removal.

In both cases a number of hyperbolas are detected at each of the object positions. There are, however, additional hyperbolas which are present and do not correspond to real objects. For each object the local velocity of propagation can be determined by

$$v = \frac{2\Delta x}{\sqrt{\beta}\Delta t} \tag{21}$$

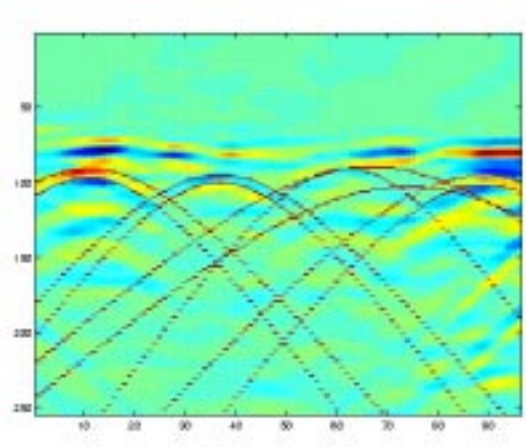

Figure 10. Detected Hyperbolas in Mean-Removed Background

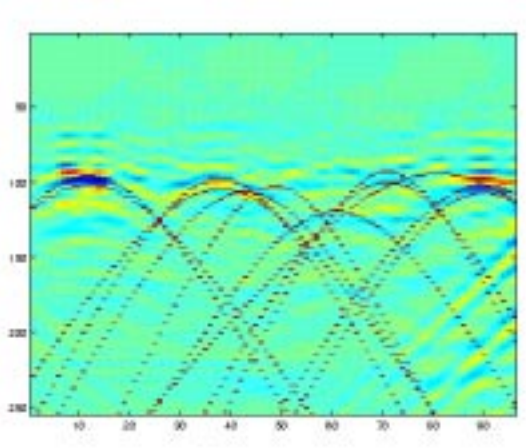

Figure 11. Detected Hyperbolas RLS-Removed Background

and the depth:

$$z = v\sqrt{\alpha} \tag{22}$$

where Δx is the horizontal distance between two sample points (the horizontal scanning step), Δt is the difference in time between two sample points (the inverse of the sampling frequency). Table 1 compares velocity, depth and eccentricity for the data before and after adaptive clutter background removal.

Table 1. Feature Comparison Between Mean-Removed and RLS-Processed Data

	Raw Data			Processed Data		
	Depth	Velocity	Eccentricity	Depth	Velocity	Eccentricity
PMA-3	4.7 cm	5.7e+7 m/s	20.5	5.6 cm	6.9e+7 m/s	19.8
Sphere	6.5 cm	6.4e+7 m/s	21.0	6.1 cm	7.1e+7 m/s	19.9
Rock	4.9 cm	6.7e+7 m/s	20.8	6.4 cm	6.5e+7 m/s	19.1
PMA-1	8.1 cm	7.0e+7 m/s	23.1	5.6 cm	7.2e+7 m/s	19.8

It is seen that, with the RLS-processed data, the estimated depth is approximately 5cm for the mines, which is close to the correct value, and the velocity estimates for the mines are approximately identical. Finally, the eccentricity is almost identical for all the objects.

This latter observation, the similarity of hyperbolic eccentricities for all targets, actually mitigates *against* using hyperbolic parameters for target discrimination. It is clear that selecting classification features based upon these parameters will not lead to efficient class discrimination.

3.2.2. Target class discrimination

Considering the above observation, van Kempen[15] then applied a multiple discriminant analysis based upon *Wilks' Lambda*[20–22] to the RLS-processed TUI data, using time, frequency and wavelet-domain features.[23] In order to compare the results for both types of data, an estimate is made of how well the selected features are clustered within each of the classes separately, and how effective those features are in separating the classes.

The selection of the best features out of the larger feature vectors, composed of all the data samples in the time, frequency and wavelet domains, is based on the estimation of Wilks' Lambda. This entity is defined as follows:

$$\lambda = \frac{det\left[\sum_{j=1}^{N}\sum_{i=1}^{n_j}\left(X_{ij}-\bar{X}_j\right)\left(X_{ij}-\bar{X}_j\right)^T\right]}{det\left[\sum_{j=1}^{N}\sum_{i=1}^{n_j}\left(X_{ij}-\bar{X}\right)\left(X_{ij}-\bar{X}\right)^T\right]} \tag{23}$$

where:

X_{ij}	Feature i in class j
n_j	Number of features in class j
$\bar{X}$	Overall feature mean
$\bar{X}_j$	Feature mean for class j
N	Number of classes

In this equation the denominator represents the determinant of the *Within Class Scatter Matrix*. This value will express how well the selected features are clustered within each of the classes separately. A small value of the denominator will represent a well clustered feature set. The numerator represents the determinant of the *Total Scatter Matrix*. This value will express how much the combined feature set is extended over the feature space. A large value can be interpreted as the fact that the distance between the class means will be large. The actual comparison between the raw and RLS-processed data will be made based upon two items: the *clustering* within a class, and the *separability* between classes.

For the clustering within a class, the assumption is made that the values of the selected features are conform to a Gaussian distribution. The *Covariance Matrix* (Co_j) of these selected features for class j can be expressed as:

$$Co_j = \sum_{i=1}^{n}\left(X_{ij}-\bar{X}_j\right)\left(X_{ij}-\bar{X}_j\right)^T \tag{24}$$

If the features are not well clustered the feature cloud will have an elongated shape in the feature space. On the other hand, if the features are well separated the feature cloud will be more spherical in shape.

Table 2 shows the comparison results, based on the defined values, for time, frequency and wavelet features separately, or when using all (combined) features. The clustering within the class is for the three objects (mine, sphere and rock) in most of the cases better in the RLS-processed data than in the raw data. Finally the classes are better separated using the RLS-processed data.

Table 2. Comparison results based on feature selection

	Raw Data				Pre-processed Data			
	Clustering (λ_1/λ_2)			Separability	Clustering (λ_1/λ_2)			Separability
	Mine	Sphere	Rock		Mine	Sphere	Rock	
Time	1.45	3.96	3.06	5.76	1.06	4.29	1.23	8.14
Freq	3.33	3.19	2.83	4.47	1.99	2.74	2.67	3.31
Wavl	3.21	2.65	1.38	2.77	2.82	2.68	2.49	4.23
All	16.42	21.52	4.46	1.19	2.17	1.67	2.67	6.85

4. CONCLUSIONS

This paper describes system-identification-based methods of characterizing and removing background clutter from a GPR signal. The methods were shown to provide quantifiable improvement in feature extraction applied to the detection of non-metallic antipersonnel land mines.

ACKNOWLEDGMENTS

The authors wish to express their gratitude to the EU Humanitarian Demining Program ESPRIT, Project 29902 DEMINE, which provided funding for this effort.

REFERENCES

1. "Basic fact sheet, UN demining data base," 1998. `http://www.un.org/Depts/dha/mct/facts.htm`.
2. B. of Political-Military Affairs, "Hidden killers." U.S. Dep't of State Publication 10575, September 1998. `http://www.state.gov/www/global/arms/rpt\_9809\_demine\_toc.html`.
3. E. Newsom, "On-the-record briefing on *Hidden Killers* report on humanitarian de-mining," tech. rep., September 1998.
4. I. Bottiglero, *120 Million Landmines Deployed Worldwide: Fact or Fiction?*, Pen & Sword Books, Ltd., London, U.K., 200.
5. I. of Electrical Engineers, *Proc. IEE/EUREL Conf. Detection of Abandoned Land Mines, Conf. Pub. No. 431*, IEE, October 1996.
6. I. of Electrical Engineers, *Proc. IEE/EUREL Conf. Detection of Abandoned Land Mines, Conf. Pub. No. 458*, IEE, October 1998.
7. J. M. U. Humanitarian Demining Center, *Sustainable Humanitarian Demining: Trends, Techniques and Technologies*, Mid Valley Press, Vienna, Virginia, 1998.
8. A. C. Dubey, R. L. Barnard, and J. E. McFee, *Detection and Remediation Technologies for Mines and Minelike Targets*, vol. 2765, SPIE Proceedings, 1996.
9. A. C. Dubey and R. L. Barnard, *Detection and Remediation Technologies for Mines and Minelike Targets II*, vol. 3079, SPIE Proceedings, 1997.
10. A. C. Dubey, J. F. Harvey, and J. T. Broach, *Detection and Remediation Technologies for Mines and Minelike Targets III*, vol. 3392, SPIE Proceedings, 1998.
11. A. C. Dubey, J. F. Harvey, J. T. Broach, and R. E. Dugan, *Detection and Remediation Technologies for Mines and Minelike Targets IV*, vol. 3710, SPIE Proceedings, 1999.
12. L. Ljung, *System Identification: Theory for the User*, Prentice-Hall, Englewood Cliffs, NJ, 1987.
13. S. Vitebskiy and L. Carin, "Resonances of perfectly conducting wires and bodies of revolution buried in a lossy dispersive half-space," *EEE Trans. Ant. Prop* **44**, pp. 1576–1583, December 1996.
14. S. Vitebskiy, L. Carin, M. A. Ressler, and F. H. Le, "Ultra-wideband, short-pulse ground-penetrating radar: Simulation and measurement," *IEEE Trans. Geoscience and Remote Sensing* **35**, pp. 762–772, May 1997.
15. J. W. Brooks, L. van Kempen, and H. Sahli, "Ground penetrating radar data processing: Clutter characterization and removal," Tech. Rep. IRIS-TR-0059, Vrije Universiteit Brussel, November 1999.
16. T. C. Hsia, *System Identification*, Lexington Books, Lexington, MA, 1976.
17. G. H. Golub and C. F. V. Loan, *Matrix Computations*, Johns Hopkins University Press, Baltimore, 3rd ed., 1996.
18. A. Swami and J. M. Mendel, "Identifiability of the ar parameters of an arma process using cumulants," *IEEE Trans. Automatic Control* **37**, pp. 268–273, February 1992.
19. S. Haykin, *Adaptive Filter Theory*, Prentice-Hall, Englewood Cliffs, NJ, 3rd ed., 1996.
20. R. O. Duda and P. E. Hart, *Pattern Classification and Scene Analysis*, Wiley Interscience, 1973.
21. S. Wilks, *Mathematical Statistics*, John Wiley, 1962.
22. L. van Kempen, E. Nyssen, H. Sahli, and J. Cornelis, "Pattern recognition experiments for ultra-sonic and radar ap-mine detection," *Sustainable Humanitarian demining: Trends, Techniques & Technologies* , pp. 297–304, 1999.
23. L. van Kempen, H. Sahli, E. Nyssen, and J. Cornelis, "Signal processing and pattern recognition methods for radar ap mine detection and identification," *MD'98: IEE/EUREL Second International Conference on the detection of abandoned landmines, Edinburgh, UK* , pp. 81–85, October 1998.